Climatology of Arctic and Antarctic Polar Vortices Using Elliptical Diagnostics

DARRYN W. WAUGH*

Meteorology CRC, Monash University, Clayton, Victoria, Australia

WILLIAM J. RANDEL

NCAR, Boulder, Colorado

(Manuscript received 2 December 1997, in final form 11 July 1998)

ABSTRACT

The climatological structure, and interannual variability, of the Arctic and Antarctic stratospheric polar vortices are examined by analysis of elliptical diagnostics applied to over 19 yr of potential vorticity data. The elliptical diagnostics define the area, center, elongation, and orientation of each vortex and are used to quantify their structure and evolution. The diagnostics offer a novel view of the well-known differences in the climatological structure of the polar vortices. Although both vortices form in autumn to early winter, the Arctic vortex has a shorter life span and breaks down over a month before the Antarctic vortex. There are substantial differences in the distortion of the vortices from zonal symmetry; the Arctic vortex is displaced farther off the pole and is more elongated than the Antarctic vortex. While there is a midwinter minimum in the distortion of the Antarctic vortex, the distortion of the Arctic vortex increases during its life cycle. There are also large differences in the interannual variability of the vortices: the variability of the Antarctic vortex is small except during the spring vortex breakdown, whereas the Arctic vortex is highly variable throughout its life cycle, particularly in late winter. The diagnostics also reveal features not apparent in previous studies. There are periods when there are large zonal shifts (westward then eastward) in the climatological locations of the vortices: early winter for the Arctic vortex, and late winter to spring for the Antarctic vortex. Also, there are two preferred longitudes of the center of the lower-stratospheric Arctic vortex in early winter, and the vortex may move rapidly from one to the other. In the middle and upper stratosphere large displacements off the pole and large elongation of the vortex are both associated with a small vortex area, but there is very little correlation between displacement off the pole and elongation of the vortex.

1. Introduction

The circulation of the winter stratosphere is dominated by a large cyclonic vortex centered near the winter pole, and changes in the circulation are generally related to changes in shape or location of this polar vortex. Historically the evolution and variability of the stratospheric circulation has been examined by analyzing the zonal (planetary) wave structure through a Fourier decomposition along latitude circles (e.g., Randel 1988; Hirota et al. 1990; Shiotani et al. 1990; Shiotani et al. 1993; Manney et al. 1991). In this study we use a set of vortex-oriented diagnostics, the so-called elliptical diagnostics (Waugh 1997; hereafter W97), as an alternative to the above Eulerian framework.

The elliptical diagnostics (EDs) of isopleths of quasi-conservative tracers, such as potential vorticity (PV) or long-lived trace constituents, define the area, center, aspect ratio, and orientation of the polar vortices (see next section for details). The EDs can be considered as an extension of the widely used area diagnostic (e.g., Butchart and Remsburg 1986; Baldwin and Holton 1988; O'Neill and Pope 1990). The area enclosed by contours at the edge of a vortex quantifies the size of the vortex and enables the formation and breakup of vortices to be examined. Similarly, the centroid of these contours quantifies the movement of the vortex, while the aspect ratio and orientation quantifies the elongation and rotation of the vortex. Hence, the EDs enable the structure and evolution of the polar vortices to be concisely summarized and quantified.

In this study, we calculate the EDs of both the Arctic and Antarctic vortices using PV on isentropic surfaces from over 19 yr of meteorological analyses (October 1978 to April 1998). These diagnostics are then used

* Current affiliation: Department of Earth and Planetary Science, Johns Hopkins University, Baltimore, Maryland.

Corresponding author address: Dr. Darryn W. Waugh, Department of Earth and Planetary Sciences, Johns Hopkins University, 320 Olin Hall, 3400 N. Charles Street, Baltimore, MD 21218.
E-mail: waugh@jhu.edu

to examine the climatological structure and interannual variability of both vortices.

As mentioned above, the structure of the stratosphere has historically been analyzed by examining the zonal wave structure (e.g., amplitude and phase of zonal waves). The relationship between the EDs and the zonal wave diagnostics has been discussed by W97, where it was shown that although qualitative information about the structure and movement of the polar vortices may be inferred from the zonal wave diagnostics, it is difficult to extract quantitative information. Furthermore, it was shown that during periods when the flow (vortex) is far from zonal symmetry it is difficult to even extract qualitative information about the vortex structure from these linear diagnostics. In appendix A, the two sets of diagnostics are compared using meteorological analyses for two different periods; these comparisons illustrate the similarities and differences between the two sets of diagnostics.

The data used and analysis procedure are described in the following section. The climatological structure of the vortices is then examined in section 3. In section 4 the distribution of the individual diagnostics, and in particular the interrelationships between the size, position, and distortion of the vortices, are examined. The interannual variability of the vortices is examined in section 5, including an examination of the variability in the timing of the breakdown of the vortices. The variability of the Arctic vortex during midwinter is also examined, by isolating periods when the vortex is either far from or close to zonal symmetry (the former are associated with warming events). Concluding remarks are given in section 6.

2. Data and analysis procedure

a. Elliptical diagnostics

The EDs are described in detail in W97, and only a brief description is given here. The EDs of a contour are obtained by fitting an ellipse to the contour and then determining several parameters of the ellipse, in particular, the equivalent latitude φ_E (the latitude of a zonal circle that encloses the same area), latitude and longitude of the center (φ_C, λ_c), aspect ratio δ, and orientation α of the ellipse. In addition, the mean-square displacement ϵ of the contour from the ''equivalent'' ellipse (the ellipse with the same EDs as the contour) can be calculated from a contour integral expression; this provides a measure of how good the elliptical fit is to the contour. By calculating the EDs of contours of quasi-conservative tracers (e.g., PV or long-lived chemical species such as nitrous oxide, N_2O) within the region of steep meridional gradients at the edge of the vortex (the vortex edge region) it is possible to define the EDs of the vortex.

The equivalent latitude φ_E (or area) of PV contours has been widely used as a diagnostic of the structure of the stratosphere (e.g., Butchart and Remsburg 1986; Baldwin and Holton 1988; O'Neill and Pope 1990) and has been used to examine the formation and decay of polar vortices, as well as the occurrence of vortex erosion events. The diagnostics φ_C and λ_c quantify the location of the vortex (in particular, $\Delta\varphi_C = 90 - |\varphi_C|$ measures the displacement of the vortex off the pole), δ measures the elongation of the vortex ($\delta \geq 1$; $\delta = 1$ corresponding to a circular vortex), and α the orientation of the vortex (relative to the Greenwich meridian).

In W97 the EDs of the polar vortices were determined using N_2O data from a general circulation model. Here we calculate the EDs of the observed vortices using PV from meteorological analyses.

b. Data

The PV data used is derived from daily stratospheric geopotential height analyses from the U. S. National Centers for Environment Prediction (NCEP), formerly called the National Meteorological Center (NMC), for the period October 1978 to April 1998. [Note that the data used are the original NCEP stratospheric analyses (Gelman et al. 1986) and not the NCEP reanalyses described in Kalnay et al. (1996).] The PV on pressure surfaces is calculated from winds and temperatures derived from the geopotential height analyses and is then interpolated to the specified isentropic surfaces. As the magnitude of PV increases rapidly with height, we use the modified PV of Lait (1994)

$$\mathrm{PV} = -g(\zeta + f)\frac{\partial\theta}{\partial p}\left(\frac{\theta}{\theta_0}\right)^{-9/2},$$

where standard notation is used and $\theta_0 = 420$ K is the reference potential temperature, to reduce this effect. With this definition, PV has a similar range of values at all θ levels. Our analysis focuses on the 440, 500, 600, 850, 1100, and 1300 K isentropic surfaces (corresponding to altitudes near 18, 20, 25, 32, 38, and 41 km).

The dataset used to generate the PV is that archived from a previous, unrelated study in which the data were truncated to zonal wavenumber 4 on a 4.5° latitude grid. This truncation was used in this previous study to provide global PV analyses free from the effects of satellite orbits and tropical wind discontinuities.

In appendix B, the sensitivity of the EDs to this spatial truncation is examined by comparing the EDs derived from these PV analyses with those derived from untruncated NCEP analyses, for the Northern Hemisphere in January 1992. The sensitivity of the EDs to the source of the meteorological data is also examined by comparing the NCEP-based EDs with those calculated using PV from two other meteorological analyses. This comparison (and other case studies, not shown) indicates that, although there are differences between the EDs from the truncated and untruncated NCEP analyses,

TABLE 1. Value of PV contour (in PVU) used to define the edge of the polar vortex in the Southern (SH) and Northern (NH) Hemispheres.

Level	SH	NH
1300 K	15	17
1100 K	19	21
850 K	27	25
600 K	29	27
500 K	27	25
440 K	23	23

these differences are small and similar to the differences between the EDs using PV from different analyses. In other words, we feel that the truncation will not significantly effect the climatology of the EDs and that any differences that it may cause are likely to be similar to the differences between climatologies using PV from different meteorological analyses.

c. Vortex edge

The EDs are calculated for 15 values of PV ($|PV| = 11, 13, \ldots, 39$ potential vorticity units (PVU); 1 PVU $= 10^{-6}$ K s^2 kg^{-1} for both hemispheres on six isentropic surfaces spanning the lower to upper stratosphere (440–1300 K). When there are multiple contours for a given value of PV, only the contour with largest area is used to derive the EDs; that is, small contours (''blobs'') surrounding the vortex are not included in the integrals used to calculate the EDs (see W97 for discussion). Note that occasionally the Arctic vortex splits into two large fragments (e.g., wave-2 warmings), and although the EDs can be calculated for each fragment we focus here only on the larger of the fragments.

Although the EDs are calculated for 15 PV contours, we concentrate on the EDS for a single contour that represents the vortex ''edge.'' For given isentropic surface and hemisphere, we use a fixed value of PV to define the vortex edge for all days in the dataset. This value is determined by calculating the mean PV of the location of the maximum meridional PV gradients ($\partial PV/\partial \varphi_E$) over all winters (December–February in Northern Hemisphere and June–August in Southern Hemisphere). The values of PV calculated from this analysis are given in Table 1. An alternative to using a fixed PV value to define the vortex edge for all days is to define the vortex edge on a daily basis by, for example, the location of the strongest latitudinal gradient on that day (e.g., Nash et al. 1996). However, the EDs (other than φ_E) are not sensitive to the PV contour used for contours within the vortex edge region (see W97), and the difference in EDs using the two definitions of the vortex edge are generally small.

This is illustrated in Fig. 1, which compares φ_E and φ_C, on the 850 K surface during the 1991/92 northern and 1991 southern winters, for the PV value listed in Table 1 (thick solid curve) and the location of maximum PV gradient (thin solid curve).[1] There are only small differences between the two edge definitions, except during the periods when the vortices are forming or breaking down (during which time there are only weak meridional PV gradients). The differences are larger in the southern fall and spring, when there are significant changes in the values of PV within the region of strong gradients at the edge of the Antarctic vortex during these periods. Because of this, care is required when interpreting diagnostics of the area of the Antarctic vortex during these periods. Although there are differences in the vortex area between the two edge definitions, there is excellent agreement in φ_C (and the other EDs, not shown). Hence, during the period when a strong vortex exists (e.g., October–March in the Northern Hemisphere and April–October in the Southern Hemisphere) the choice of vortex edge will not impact the calculated EDs.

3. Climatology

We now consider the climatological structure of the polar vortices. The climatology is constructed by averaging over each calendar day the EDs for each PV contour. We present first the climatological φ_E for all PV contours and then examine the climatologies of the other EDs for the edge contour defined in section 2 (see Table 1).

Since first being used in Butchart and Remsburg (1986), who examined φ_E during the 1982/83 Arctic winter, several studies have examined the seasonal evolution of φ_E for each year in a multiyear dataset. For example, Baldwin and Holton (1988) examined φ_E at 850 K in the Northern Hemisphere for the years 1964–82, O'Neill and Pope (1990) examined φ_E at 850 K in both the Northern and Southern Hemispheres for the years 1979–88, Manney et al. (1994) examined φ_E at 465 K in the Northern Hemisphere for the years 1979–94, and Manney et al. (1995) examined φ_E at 465 and 840 K in the Northern and Southern Hemisphere for more recent years (1991–94). In contrast, here we examine the mean φ_E over 19 southern and 20 northern winters rather than φ_E of individual winters. [Note that a recent study by Baldwin and Dunkerton (1998) examined a climatology of φ_E for 32 yr of Northern Hemisphere PV at 600 K.]

Figure 2 shows the temporal evolution of climatological φ_E on the 500, 850, and 1300 K surfaces for the Southern (left column) and Northern (right) Hemispheres (the thick curves correspond to the vortex edge contours listed in Table 1). These plots show the same

[1] Note that here (and, unless otherwise stated, in the remainder of the paper) a Gaussian time filter with half-width of 2 days has been applied to the data, with the effect of smoothing the highest-frequency daily variations. Also, φ_C and the other EDs are not shown if $|\varphi_E| > 85°$ (i.e., the vortex area must be larger than 5° equivalent latitude).

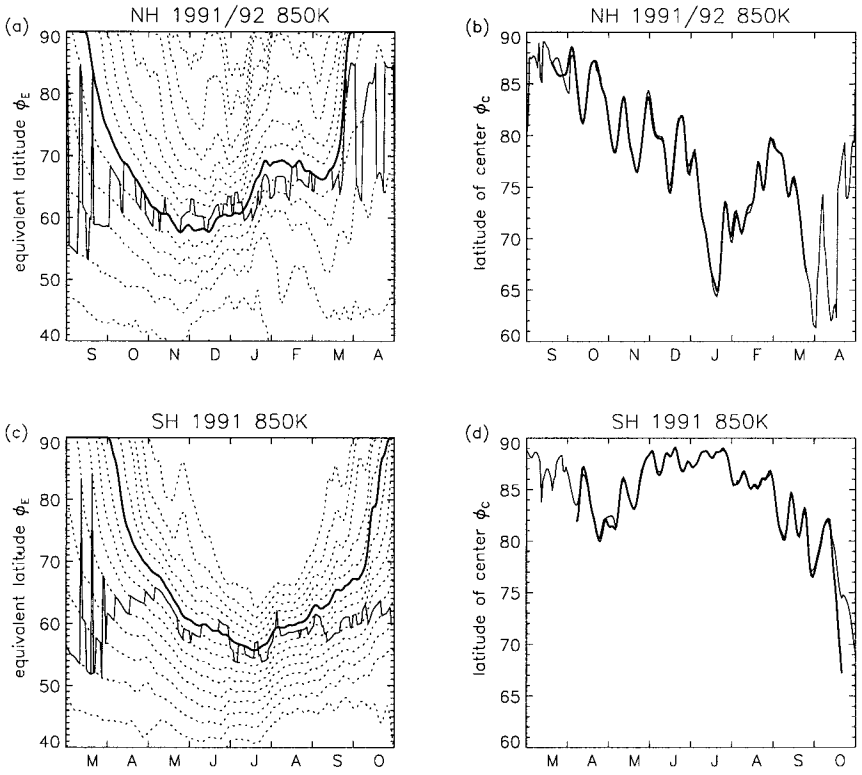

FIG. 1. Variation of φ_E and φ_C at 850 K in (a), (b) Northern Hemisphere for 1991/92 winter and (c), (d) Southern Hemisphere for 1991 winter. All PV contours are shown in (a) and (c), while only edge contours are shown in (b) and (d). The thick solid curves correspond to edge given in Table 1, while the thin solid curve corresponds to the PV at the maximum meridional gradient.

general features noted in the above studies. There is, in both hemispheres and at all levels, an increase in φ_E of PV contours and formation of a region of steep meridional PV gradients at high latitudes (vortex formation) in autumn/early winter and a decrease in φ_E and PV gradients (vortex demise) in late winter/spring.

The region of steep gradients form first at upper levels, with a lag of around 2 months between formation at 1300 K (March in the Southern and September in the Northern Hemisphere) and at 500 K (May in the Southern and November in the Northern Hemisphere). There is a similar difference in the time at which the Antarctic vortex attains its maximum areal extent (e.g., late June at 1300 K and late August at 500 K), but a smaller time lag for the Arctic vortex (mid-December at 1300 K and mid-January at 500 K). The vertical variation in the timing of the decay of the steep gradients is much smaller than that for the formation, with the decay occurring at all levels within a month. While the steep gradients form at roughly the same season in each hemisphere, the decay occurs earlier in the Northern Hemisphere; that is, the Arctic vortex has a shorter life span than the Antarctic vortex.

The variation of the size of the Arctic vortex at 1300 K differs qualitatively from lower levels and from all levels of the Antarctic vortex. At 1300 K, there is not a monotonic decrease in size of the Arctic vortex after it has attained its maximum size; that is, there is a ''bite'' out of φ_E at 1300 K in January and February. This is due to the occurrence of midwinter events in which the Arctic vortex breaks down in the upper stratosphere (see section 5a below).

During midwinter, the size of both vortices increases with θ (altitude) but the increase for the Antarctic vortex is much larger than that for the Arctic vortex. This difference is shown clearly in Fig. 3, where the variation of $|\varphi_E|$ with θ is shown for the edge PV contour (Table 1) for the July mean Antarctic (solid) and January mean Arctic (dashed) vortices. The Antarctic vortex is larger throughout the stratosphere, with the largest difference in the upper stratosphere (at 1300 K, the area of the Antarctic vortex is over twice that of the Arctic vortex). For each vortex the θ dependence of φ_E at the vortex edge changes during the vortex life cycle. The increase of $|\varphi_E|$ with θ decreases through the winter, and by spring there is no significant vertical variation in the size of either vortex. Note again the sensitivity to PV contours used in southern spring: using the location of the maximum PV gradients the size of the Antarctic vortex gen-

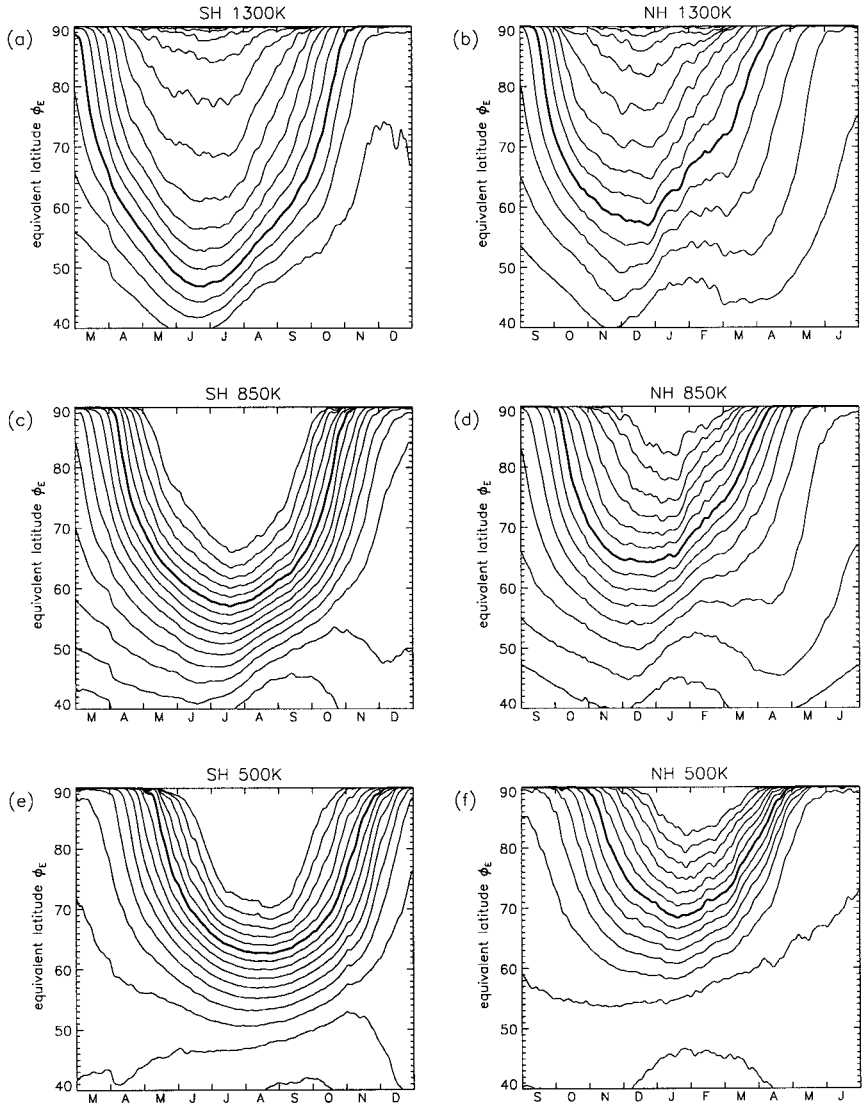

FIG. 2. Temporal evolution of climatological φ_E for (left) Southern and (right) Northern Hemisphere at (upper) 1300 K, (middle) 850 K and (lower) 500 K. Contour interval is 2 PVU, and thick curves correspond to PV values in Table 1.

erally decreases with height in late spring (November) [e.g., Mechoso (1990); Lahoz et al. (1996)].

We now consider the climatological structure of the other EDs. Figure 4 shows the seasonal and vertical variation of the mean φ_E, $\Delta\varphi_C$, λ, and δ for the Antarctic (left column) and Arctic (right) vortices. Note that additional smoothing, using a Gaussian time filter with half-width of 10 days (this is similar to moving monthly means), has been used in these plots. We first consider the structure and evolution of the Antarctic vortex, and then that of the Arctic vortex.

a. Antarctic vortex

Figure 4a shows the variation of φ_E at the edge of the Antarctic vortex. This plot shows the same features discussed above: area increases in the upper stratosphere around 2 months before the lower stratosphere (March compared with May), similar lag in occurence of maximum area during winter, very little variation with altitude in the decrease in area, and area increasing with θ except during late winter to spring (September–October) when there is only a small θ variation.

The movement of the Antarctic vortex off the pole is shown in Fig. 4c. Through most of its life cycle the vortex is centered near the pole ($\Delta\varphi_C \sim 4°$ to 6°); however, during spring the vortex moves well off the pole ($\Delta\varphi_C > 10°$). This movement off the pole in October is linked with the intensification of a quasi-stationary anticyclone (Mechoso et al. 1988; Lahoz et al. 1996) or a stationary zonal wave 1 (Randel 1988). There is a minimum in the displacement from the pole in mid-

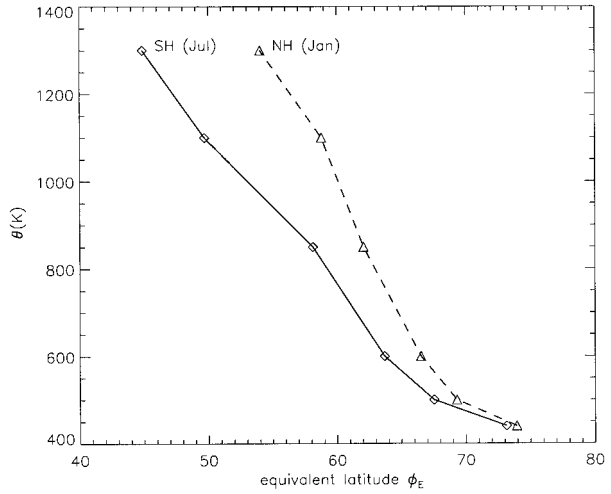

FIG. 3. Variations of φ_E at vortex edge with θ for July-mean Antarctic vortex (solid curve) and January-mean Arctic vortex (dashed).

winter ($\Delta\varphi_C \sim 3°$), and this minimum occurs at roughly the same time as the vortex is largest (minimum φ_E), that is, late June in upper stratosphere and late August in lower stratosphere. The occurrence, and timing, of the minimum displacement off the pole is consistent with the minimum of the amplitude of zonal wavenumber 1 (e.g., Randel 1988). However, in contrast to the wave-1 amplitude, there is not a local maximum in $\Delta\varphi_C$ in either early or late winter. The maximum $\Delta\varphi_C$ occurs at the end or beginning of the season rather than within each season (as for the wave-1 amplitude). As discussed in W97 the amplitude of wave 1 is affected by the meridional gradients of the field being analyzed, and so some of the seasonal changes in wave-1 amplitude are due to seasonal changes in the meridional structure of the vortex rather than changes in the location of the vortex center.

Figure 4c also shows that, except during late winter–spring, there is very little meridional tilt in the center of the Antarctic vortex. During the first half of its life cycle (April–mid-July) the Antarctic vortex tilts slightly poleward with height ($\Delta\varphi_C$ decreases by $\sim 2°$ between 440 and 1300 K), whereas during the second half of its life cycle the vortex tilts equatorward. This meridional tilt increases toward the end of winter, and in spring there is around an 8° difference in $\Delta\varphi_C$ between 1300 and 440 K.

The longitude of the Antarctic vortex center, at given θ, is relatively constant from autumn to late winter (see Fig. 4e). But during late August to early September there is westward shift (of around 30°) in the climatological location of the vortex, which is then followed in mid-September to October by a comparable eastward shift. Throughout its life cycle the vortex tilts westward with height (decreasing λ_c with θ), and the magnitude of the tilt is relatively constant (approximately 50°–70° between 440 and 1300 K), even during the shift in location between late August and October.

The vertical and temporal variation of the elongation (aspect ratio) of the Antarctic vortex is similar to that of its displacement off the pole (see Fig. 4g); that is, δ is small during winter but increases during the spring breakdown of the vortex. There is a midwinter minimum ($\delta < 1.2$), with the minimum occurring in the upper stratosphere 2 months prior to the lower stratosphere. However, the minimum in δ occurs around a month before the minimum in $\Delta\varphi_C$ (and φ_E). Also, unlike $\Delta\varphi_C$, δ is large during vortex formation, although, as discussed in section 2, δ is sensitive to the contour used to define the vortex during this period and different values may be obtained using a different definition of the vortex edge. During early and midwinter, δ is larger in the lower stratosphere than in the upper, but there is only a small vertical variation in late winter and spring.

b. Arctic vortex

We now consider the structure and evolution of the Arctic vortex. Comparing Figs. 4a and 4b we see that, as discussed above, the altitudinal and temporal variation of the size of Arctic vortex are similar to that of the Antarctic vortex, but the Arctic vortex is smaller and breaks down earlier.

Although there is qualitative agreement in the evolution of the size of the vortices, there are substantial differences in the distortion of the vortices. Whereas there are midwinter minima in $\Delta\varphi_C$ and δ for the Antarctic vortex, both quantities increase during the Arctic vortex life cycle. Also, the displacement off the pole and elongation of the Arctic vortex are much greater than the Antarctic vortex; for example, at 850 K in midwinter $\Delta\varphi_C \sim 14°$ and $\delta \sim 1.7$ for the Arctic vortex, compared with $\Delta\varphi_C \sim 4°$ and $\delta \sim 1.2$ for the Antarctic vortex.

The longitude of the center of the Arctic vortex is more variable than the Antarctic vortex, with the Arctic vortex undergoing a large shift in location (eastward then westward) in November–December, and a smaller shift in late January–early February. Note that whereas the large changes in the longitude of the Antarctic vortex occur in late winter, the corresponding large changes of the Arctic vortex are in early winter. Although the longitude of the Arctic vortex is more variable, the zonal tilt of the Arctic vortex is similar to that of the Antarctic vortex, that is, westward tilt with height of 50°–70° between 440 and 1330 K, and this tilt is relatively constant with time even when the vortex shifts westward and eastward.

The hemispheric differences in the shape and position of the polar vortices discussed above can be seen clearly in plots of the equivalent ellipses of the vortices (the ellipses with the same EDs as the vortex). Figure 5 shows polar stereographic plots of the monthly-mean equivalent ellipses at 850 K for Arctic (solid) and Ant-

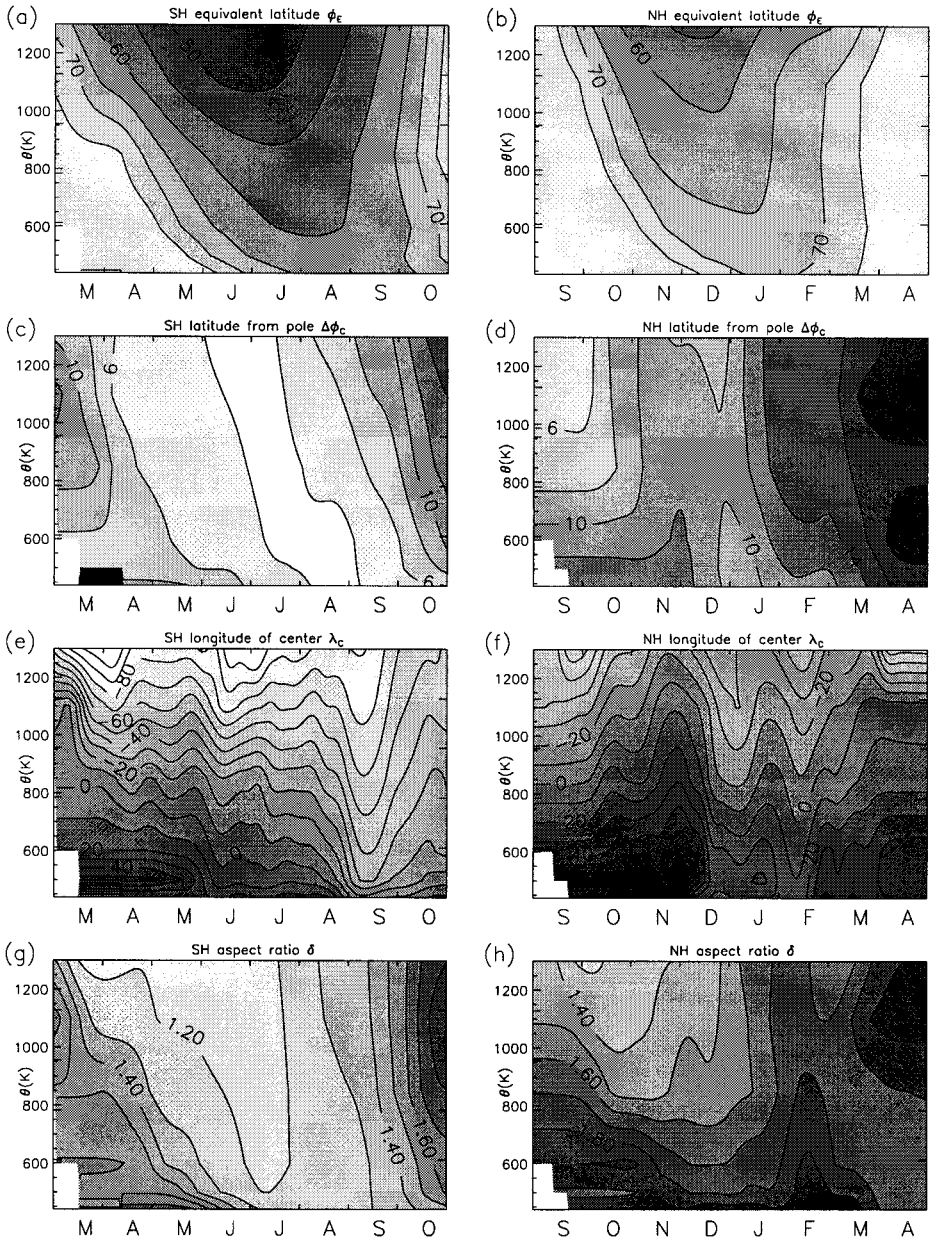

FIG. 4: Altitude–time contour plots of the climatological EDs for the (left) Antarctic and (right) Arctic vortices: (a),(b) φ_E (contour interval 5°); (c),(d) $\Delta\varphi_C$ (2°); (e),(f) λ_c(10°); and (g),(h) δ (0.1).

arctic (dashed) vortices from early to late winter; the symbols represent the center of vortices. (The months for the Arctic and Antarctic vortex are offset by 6 months so that the plots correspond to the same season). These plots clearly show that the Antarctic vortex is larger, less distorted from zonal symmetry, and has a longer life span than Arctic vortex. Figure 6 shows the equivalent ellipses at all levels for (a) July-mean Antarctic vortex and (b) January-mean Arctic vortex (the asterisks mark the center of the vortices, while the open circles mark the pole). This shows clearly the differences in the vertical structure of the vortices.

4. Distribution and interrelationship of EDs

We now examine the distribution and interrelationships of the individual EDs by analyzing two-dimensional histograms (contour plots) of pairs of EDs. The histograms are constructed for each θ level by simply counting the number of occurrences of each quantity within a certain range (a 1° bin for φ_E, for instance). Statistics are calculated using all the years of data during northern winter (December–February) and southern late winter–spring (August–October); these are the periods of strongest vortex variability. The resulting distribu-

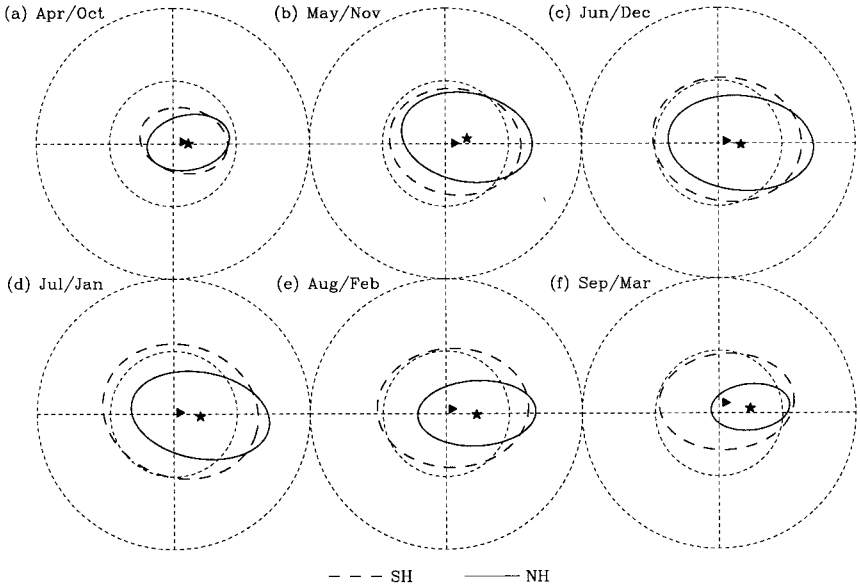

FIG. 5. Polar stereographic plots of monthly-mean equivalent ellipses at 850 K for Antarctic (Arctic) dashed (solid) curves for (a) April (October), (b) May (November), (c) June (December), (d) July (January), (e) August (February), and (f) September (March). Triangles (asterisks) represent the center of the Antarctic (Arctic) vortex.

tions are smoothed two dimensionally to a degree that removes ''spikelike'' features but retains the overall details of the distributions.

Figure 7 shows the distribution of φ_E versus $\Delta\varphi_C$ in the Northern Hemisphere, at 440 and 1100 K. These plots explore the relationship between the size of the vortex and movement off the pole. The contours show a smooth distribution of states about the time mean values discussed above. The shape of the contours indicates that there is little correlated variation between these variables in the lower stratosphere (440 K). There is, however, a notable slope in the contours at 1100 K, such that smaller vortex area (larger φ_E) is associated with movement off the pole (larger $\Delta\varphi_C$). This latter relationship is observed throughout the mid- to upper stratosphere (850–1300 K), whereas little correlation is seen over the 440–600 K levels.

Calculation of similar diagnostics for the Antarctic vortex show much less spread in values of $\Delta\varphi_C$, with $\Delta\varphi_C < 10°$ (i.e., vortex center within 10° of the pole) for 90% of the distribution. At upper levels (above 850 K) there is a slope of the $\Delta\varphi_C$-φ_E contours similar to the 1100 K Northern Hemisphere patterns in Fig. 7, showing movement of the pole correlated with smaller vortex area.

Figure 8 shows plots of φ_E versus λ_c, analyzing the relationship between the longitude of the vortex and its area, and again there is a large contrast between the

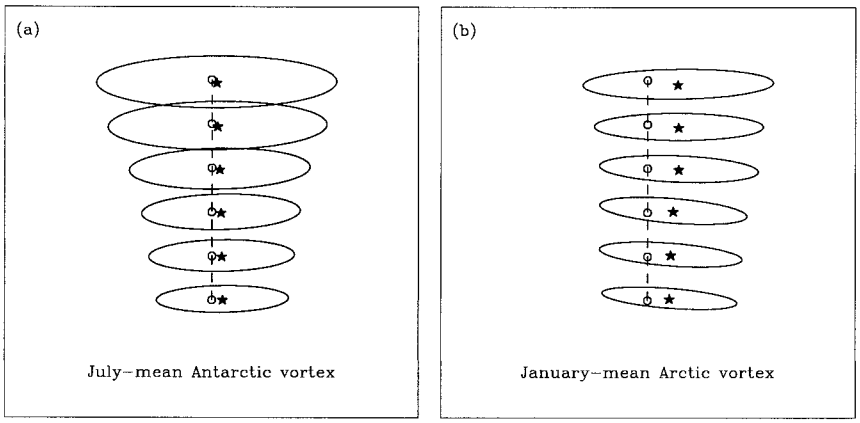

FIG. 6. Stacked plots of equivalent ellipses at each level of (a) July-mean Antarctic vortex and (b) January-mean Arctic vortex.

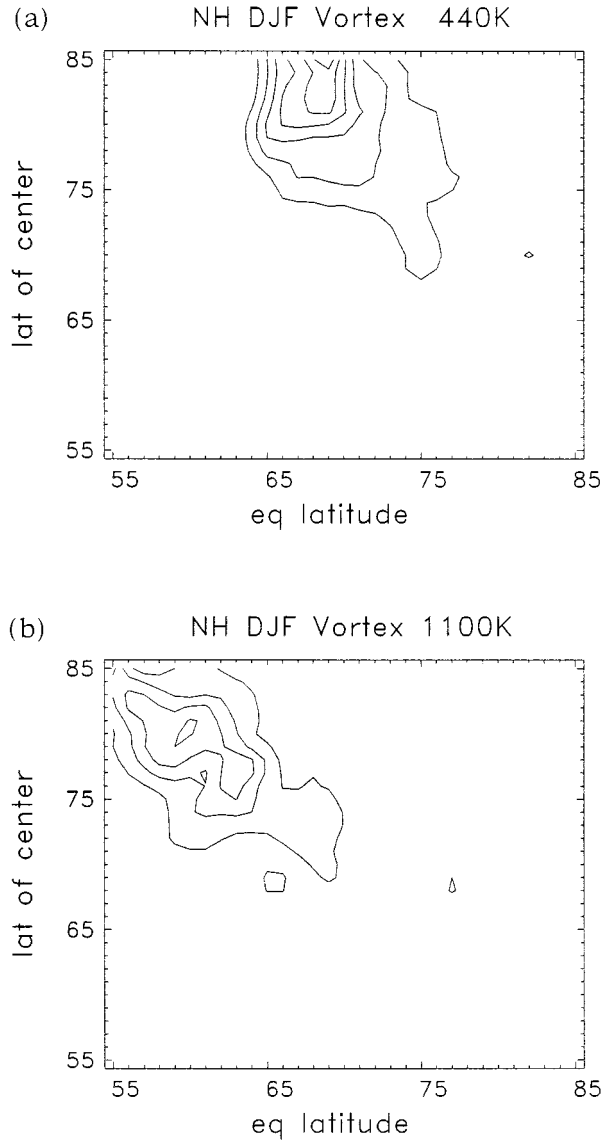

FIG. 7. Contour plot of relative frequency (two-dimensional histogram) of latitude of center φ_C vs equivalent latitude φ_E for Arctic vortex during December–February at (a) 440 and (b) 1100 K.

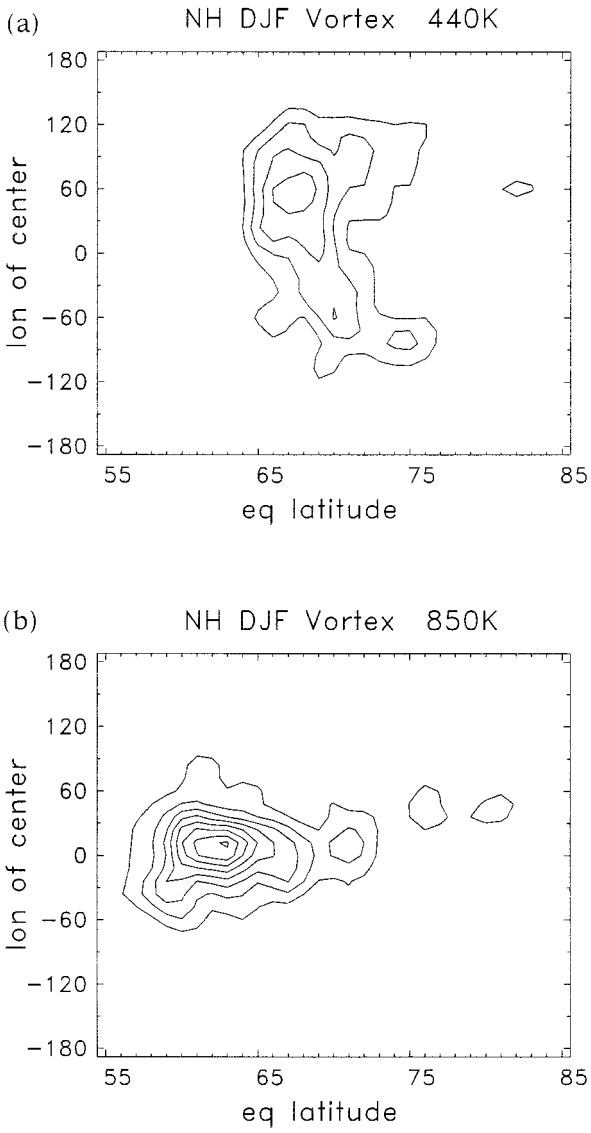

FIG. 8. Contour plot of relative frequency (two-dimensional histogram) of longitude of center λ_c vs equivalent latitude φ_E for Arctic vortex during December–February at (a) 440 and (b) 1100 K.

behavior in the Northern Hemisphere lower and upper stratosphere. At 440–600 K there is a broad distribution of λ_c, spanning longitudes approximately 90°W–120°E, whereas at 850 K (and above) there is a much narrower distribution of λ_c, which peaks near 0°.

The data at 440 K in Fig. 8 furthermore hint at a bimodal distribution in λ_c, with one maximum (mode) near 60°E and another around 60°–90°W. This bimodal structure is even more pronounced in data for December alone, as shown in Fig. 9a. One possibility is that this bimodality could arise because the vortex is in one mode in some winters, and in the other mode in different years. However, analyses of individual Decembers show this bimodality during about half of the years; see, for example, Fig. 9b, which shows the contour plot of φ_E versus λ_c for December 1994. Hence, the vortex can move from one mode to another within a single winter. Inspection of the time series of λ_c shows that rapid changes can occur at 440 K; that is, the vortex center can move from the 60°–120°E region to the 60°–90°W region in a few days (in mid-December 1994 the transition from 100°E to 100°W occurred in 3 days). Corresponding changes in λ_c can be traced to the 850 K level, but the magnitude and speed of the changes decrease with height (consistent with the decrease in spread and bimodality in the histograms at levels above 440 K). Note that during the December period the vortex is generally a single well-defined structure, and the bi-

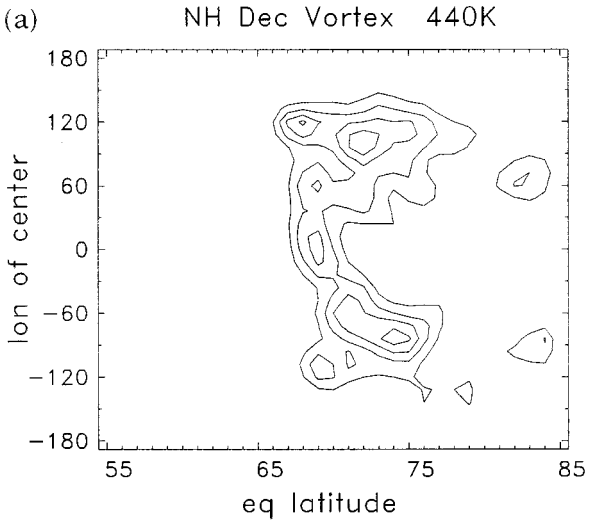

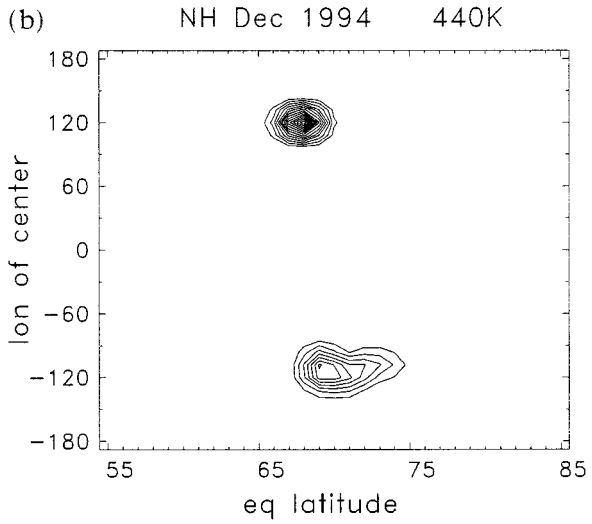

FIG. 9. As in Fig. 8 except for longitude of center λ_c vs equivalent latitude φ_E at 440 K for (a) all December data and (b) December 1994.

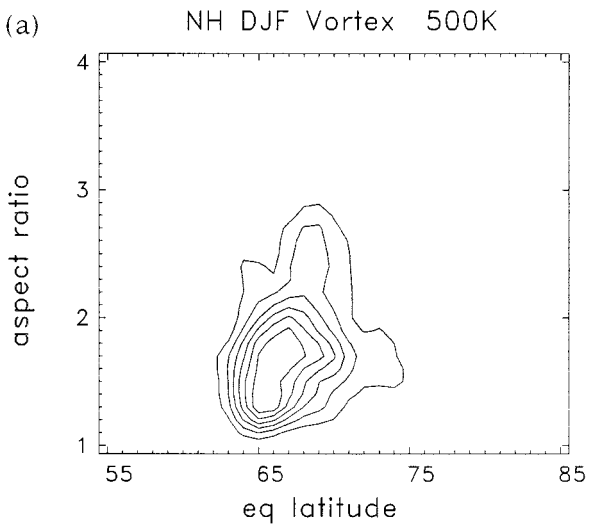

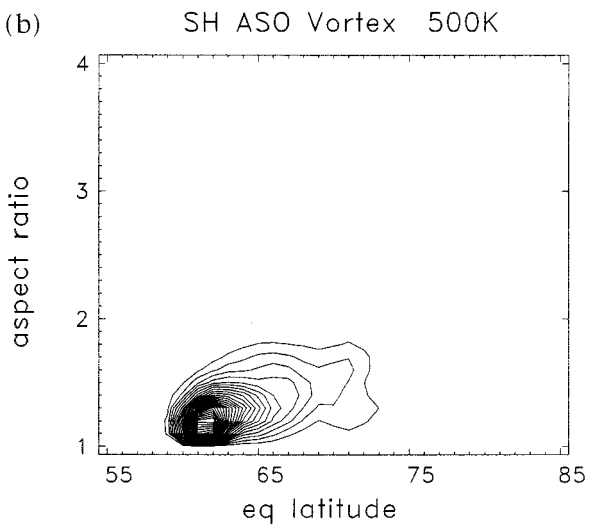

FIG. 10. Contour plot of relative frequency (two-dimensional histogram) of aspect ratio δ vs equivalent latitude φ_E for (a) Arctic vortex during December–February at 500 K and (b) Antarctic vortex during August–September at 500 K.

modality is not an artifact of picking up different centers of a split vortex.

Preliminary analysis indicates that the above shifts in λ_c may be linked to changes in the tropospheric circulation. For example, around the time of the shift in λ_c during December 1994 there was a major change in tropospheric circulation, corresponding to the onset of a strong negative phase in the tropospheric tropical/Northern Hemisphere pattern (Livezey and Mo 1987), with anomalous negative (positive) height anomalies forming over the North Pacific (North America) (NOAA 1994).

The distributions of φ_E versus λ_c in the Southern Hemisphere are qualitatively, similar to those for the Northern Hemisphere. There is a similar contrast between the lower and upper stratosphere, with a wider distribution of λ_c in the lower stratosphere. However, there is no sign of bimodal structure of λ_c at 440 K in the Southern Hemisphere.

Figure 10 shows the distributions of δ versus φ_E (in order to study the relationship between vortex area and elongation) at 500 K for both the Northern and Southern Hemispheres. There is a much wider range of δ values in the Northern Hemisphere, reflecting the more disturbed nature of the Arctic vortex. There is an overall slope to the contours in both plots in Fig. 10, showing that in both hemispheres a more elongated vortex (larger δ) is associated with a smaller vortex (larger $|\varphi_E|$). Similar distributions are found at other levels, although the

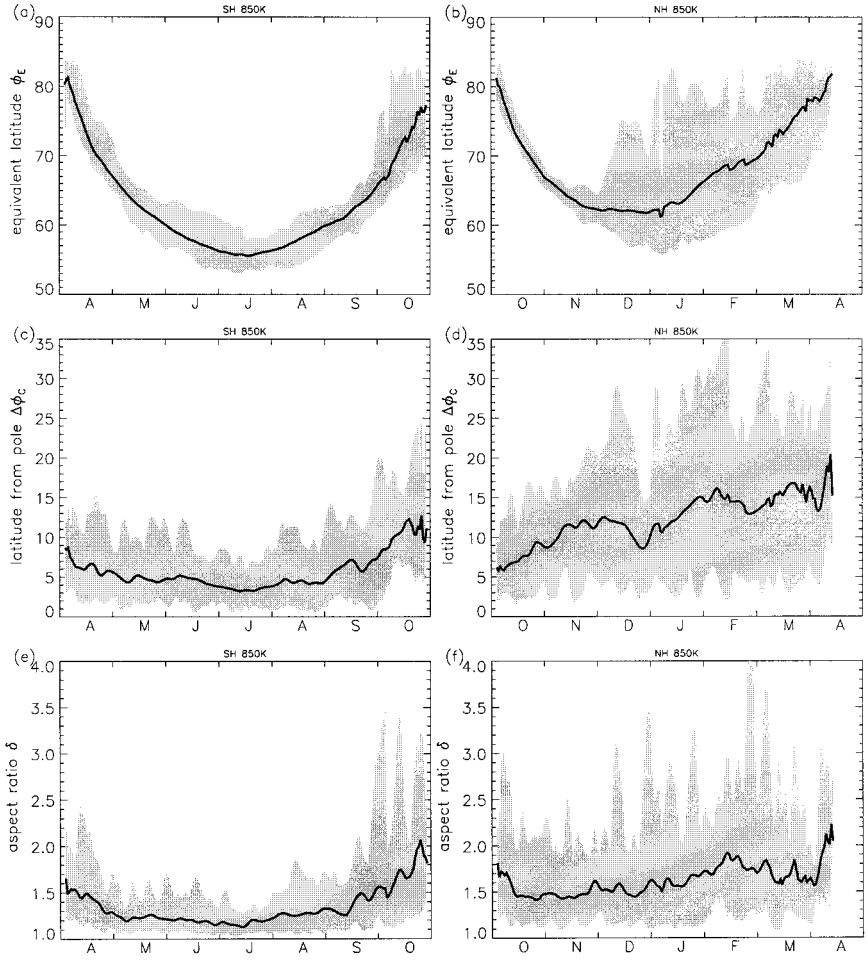

FIG. 11. Mean (solid curve) and range (shaded region) of (upper) φ_E (middle) $\Delta\varphi_C$, and (lower) δ for (left) Antartic vortex and (right) Arctic vortex at 850K.

slope of the contours varies with θ (particularly in the Northern Hemisphere).

Contour plots of other pairs of diagnostics have also been examined (not shown), and these generally show smooth distributions about the time mean values with very little correlations between the various quantities. For example, the distributions of δ versus $\Delta\varphi_C$ (vortex elongation vs latitude from the pole) only display a notable slope in the upper stratosphere (1100 K and above) of the Arctic vortex, and even then the variation of δ with $\Delta\varphi_C$ is small. So generally there is very little correlation between the elongation of the vortex (δ) and the movement of the vortex off the pole ($\Delta\varphi_C$).

5. Interannual variability

The interannual variations of the vortices are analyzed by examining, for each calendar day, both the standard deviations about the above mean values and the range of values within the 19 (southern) or 20 (northern) winters. For both vortices there are relatively small vertical variations in the interannual variability; that is, the magnitude and seasonal evolution of standard deviation of the EDs are similar for all θ.

Figure 11 shows the range of values (shaded region) and mean value (solid curve) of φ_E, $\Delta\varphi_C$, and δ for the Antarctic (left column) and Arctic (right) vortices at 850 K. These plots clearly show that the Arctic vortex is more distorted and has much larger interannual variability than the Antarctic vortex. The interannual variability of the Antarctic vortex size, location, and excentricity is very small (e.g., the standard deviation of φ_E and $\Delta\varphi_C$ is around 2°) except during the vortex formation and breakdown. On the other hand the variability of the Arctic vortex is large (the standard deviations of φ_E and $\Delta\varphi_C$ of the Arctic vortex during winter are over three times that of the Antarctic vortex), with the largest variability in late winter. The maxima in all three quantities of the Arctic vortex in mid-December and early January correspond to stratospheric warmings that occurred in the 1987/88 and 1984/85 winters, respectively.

A large amount of interannual variability of the struc-

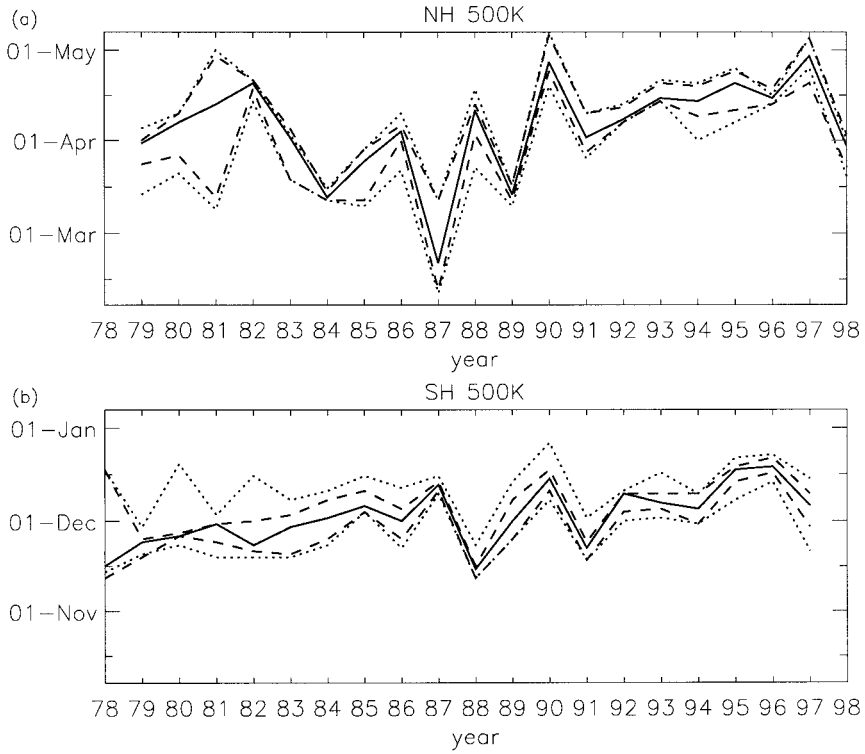

FIG. 12. Date of breakdown of (a) Arctic and (b) Antarctic vortices at 500 K for each year between 1978 and 1998. The different curves correspond to different combinations of PV values and critical values of φ_E. The solid curves correspond to $|\varphi_E| < 80°$ for PV = 19 PVU for Antarctic and 23 PVU for Arctic vortex, the dashed curves correspond to using PV values smaller or larger by 2 PVU, and the dotted curves correspond to using critical φ_E smaller or larger by 5°.

ture of both vortices during spring is related to the interannual variability in the timing of the breakdown of the vortices. Figure 12 shows the date of vortex breakdown at 500 K for the (a) Arctic and (b) Antarctic vortices for each year of the climatology. The breakdown date is defined here as the last day when $|\varphi_E|$ exceeds a critical threshold. The different curves correspond to different combinations of PV values and critical values of φ_E. The solid curves correspond to $|\varphi_E| < 80°$ for PV = 19 PVU for Antarctic and 23 PVU for Arctic vortex (these are different PV values than in Table 1 and correspond to the climatological mean PV of maximum PV gradients during late winter/spring). The dashed curves correspond to using PV values smaller or larger by 2 PVU, whereas the dotted curves correspond to using critical φ_E smaller or larger by 5°. There is some variation in the breakdown date depending on the parameters used, but the interannual and decadal varaitions are generally the same for all combinations [Also very similar dates for the Arctic vortex are obtained using the definition of Nash et al. (1996); E. Nash 1998, personal communication.]

Figure 12 shows that there is large interannual variability in the timing of the breakdown of the vortices, particularly in the Northern Hemisphere. The year-to-year variability during the late 1980s to early 1990s is larger than earlier or later periods (again this is more pronounced in the Northern Hemisphere), with suggestion of a biennel oscillation (see also Baldwin and Dunkerton 1998). Also, there appears to be a slight ''trend'' in the lifetime of both vortices, with the vortices lasting longer in more recent years.

We now consider in more detail the interannual variability of each vortex.

a. Arctic vortex

The variation of $\Delta\varphi_C$ (solid curve) and δ (dashed) at 850 K for the individual Arctic winters (December–February) from 1990/91 to 1997/98 is shown in Fig. 13. As expected from Fig. 11, there is large year-to-year variability. A lot of this variability is due to the occurrence of events where the vortex is extremely distorted (i.e., the vortex is centered well off the pole and/or is very elongated): these events do not occur every year, and the timing varies between years.

To examine the occurrence of events in which the vortex is highly distorted we isolate periods during which

$$\Delta\varphi_C > \Delta\varphi_C^{\mathrm{D}} \quad \text{or} \quad \delta > \delta^{\mathrm{D}}, \tag{1}$$

where $\Delta\varphi_C^{\mathrm{D}}$ and δ^{D} are fixed values (see below). We

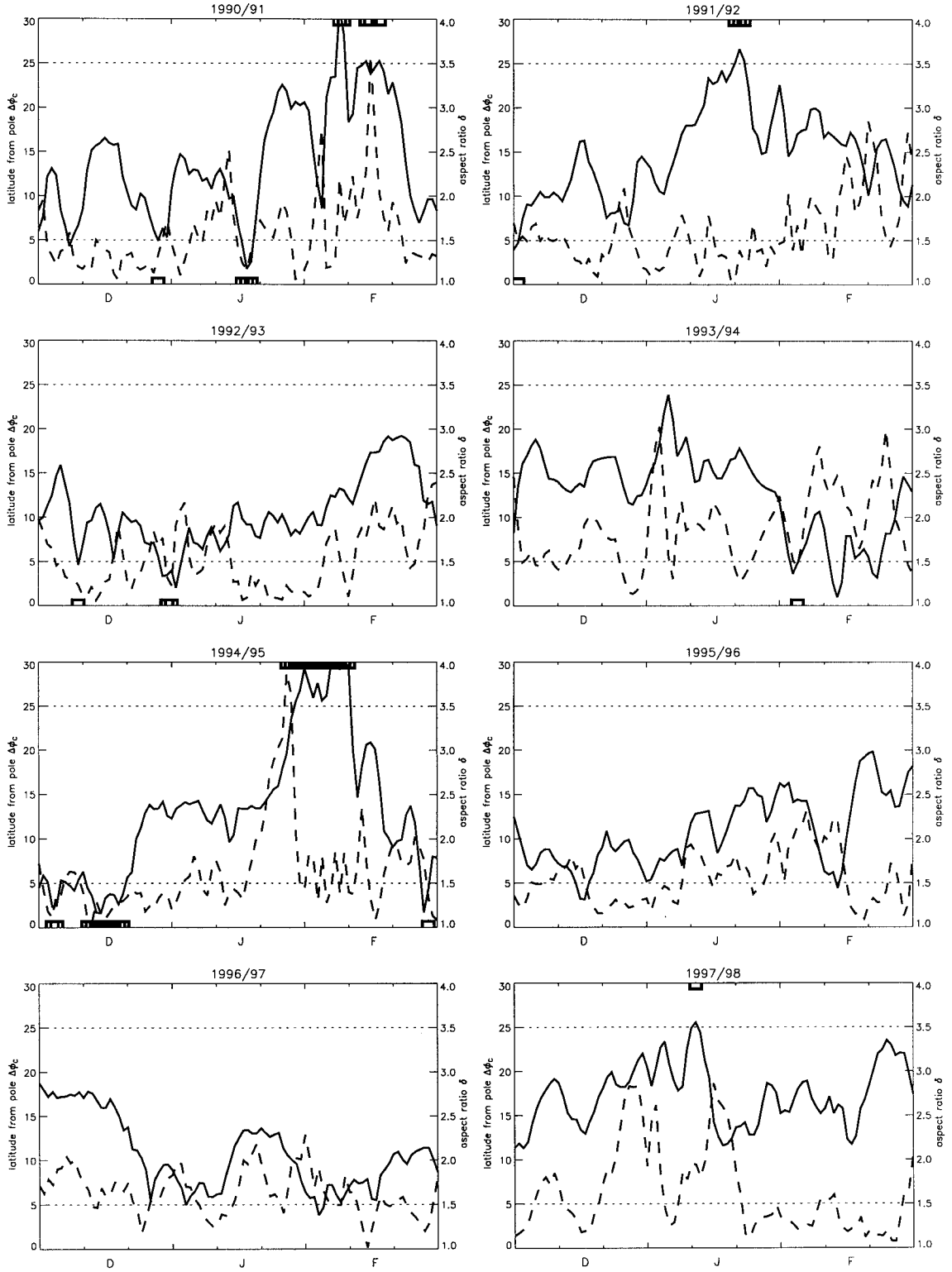

FIG. 13. Variation of $\Delta\varphi_C$ (solid curve) and δ (dashed) at 850 K during Dec–Feb for winters between 1990/91 and 1997/98. Boxes on upper (lower) axes signal the occurrence of a D (Q) vortex (horizontal dashed lines correspond to critical values used to define D and Q vortices); see text for details.

refer to vortices that satisfy (1) as distorted (D) vortices. The occurrence of a D vortex during the winters shown in Fig. 13 is marked by boxes on the upper axes of each plot; here we have used $\Delta\varphi_C^{\mathrm{D}} = 25°$ and $\delta^{\mathrm{D}} = 3.5$ in (1). Using these critical values there is a D vortex in half the winters between 1990/91 and 1997/98 (February 1991, January 1992, late January–early February 1995, January 1998). At some stage during all four events the vortex center is equatorward of 65°N (i.e., $\Delta\varphi_C$ exceeds 25°), but only in the 1991 and 1995 events is the vortex is very elongated (i.e., δ exceeds 3.5). Note that although $\Delta\varphi_C$ and δ are both large during these two events, this does not generally happen on the same day (consistent with the lack of a strong correlation between δ and $\Delta\varphi_C$ discussed in the previous section). The four D events shown in Fig. 13 correspond to major (1991) or near-major (1992, 1995, and 1998) warmings.

During periods when there is a D vortex using the above definitions there is also a decrease in vortex size (increase in φ_E) and the vortex becomes nonelliptical (an increase in ϵ) (not shown). Both changes are consistent with material being stripped from the vortex in filaments during these periods (the area decreases because air is removed in the filaments, and the filaments mean that PV contour are nonelliptical; see Figs. 2 and 3 of W97).

From Fig. 13 it can be seen that there are also periods where the vortex is close to zonal symmetry (i.e., nearly circular and centered close to the pole). We determine these periods using the criterion

$$\Delta\varphi_C < \Delta\varphi_C^{\mathrm{Q}} \quad \text{and} \quad \delta < \delta^{\mathrm{Q}} \tag{2}$$

(where $\Delta\varphi_C^{\mathrm{Q}}$ and δ^{Q} are constants). Vortices satisfying (2) are referred to as ''quiescent'' (Q) vortices. Note that whereas only one of $\Delta\varphi_C$ and δ needs to exceed critical values for the vortex to be defined as D vortex, both must be less than critical values for a Q vortex to exist. The occurrence of a Q vortex in Fig. 13 is shown by the boxes on the lower axes [here we have used $\Delta\varphi_C^{\mathrm{Q}} = 5°$ and $\delta^{\mathrm{Q}} = 1.5$ in (2)]. There is a Q vortex in four of the eight winters shown, and during two of these winters there is also another period when there is a D vortex. In other words, in the same winter the vortex can be close to zonal symmetry for some period of time and far from zonal symmetry for another period.

The frequency of D and Q vortices during each winter (DJF) is shown in Fig. 14. Days when there is a D vortex occur within a single ''event'' in each winter, and these events generally last from several days to two weeks. The Q vortices also occur during short events, although two separate events can occur in a single winter (e.g., 1990/91). It was noted above that a D and Q vortex can occur during the same winter. In fact, from Fig. 14 we see that this is generally the case: in all winters with a D vortex there is also a Q vortex except for 1981/82 and 1986/87. Because there are many winters when there are significant days of both Q and D vortices, it is difficult to define whole winters as being either Q or D. However, having said this, it is noticeable that D vortices have been rarer during the 1990s in comparison with the 1980s. Hence, during the 1980s the Arctic vortex was generally more disturbed and broke down earlier (see Fig. 12) than during the 1990s.

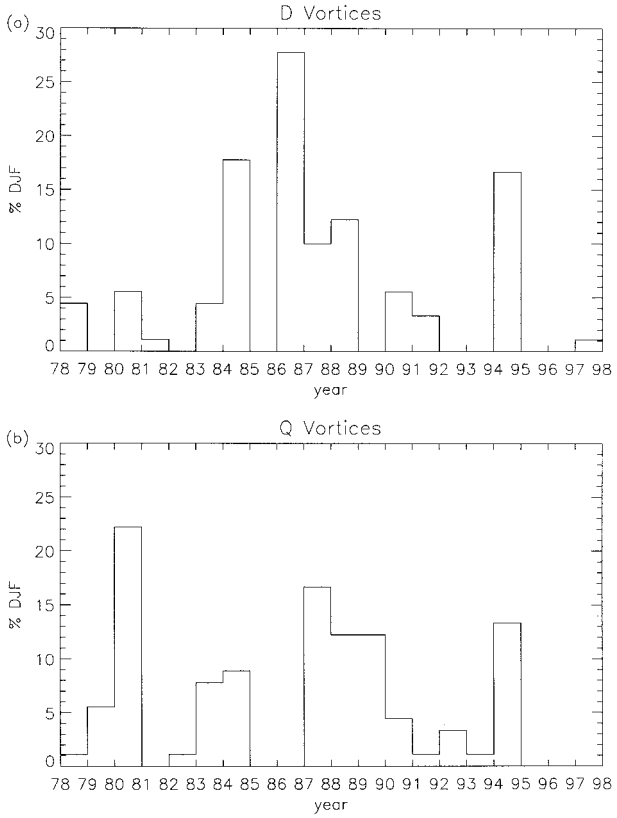

FIG. 14. The number of days when a D or Q vortex exists during each winter (DJF) between 1978/79 and 1997/98.

The above criterion have also been used to isolate D and Q vortices in the Southern Hemisphere (not shown). For the same critical values as used above, there is never a D vortex during Southern Hemisphere winter (JJA) but there is frequently a Q vortex, with the occurrence during JJA varying between 33% (1992) and 93% (1981).

The above ''extreme'' events (D or Q vortices) in the Northern Hemisphere correspond closely to the three flow regimes defined by Pierce and Fairlie (1993) (see also Pawson and Kubitz 1996). The three regimes correspond to weak zonal wind and weak wave amplitude (regime 1A), strong zonal wind and weak wave amplitude (regime 1B), and intermediate zonal wind and strong wave amplitude (regime 2). The regime 1B corresponds closely to the occurrence of a Q vortex (when the vortex is close to the pole and nearly circular there is weak wave-1 amplitude and a strong jet), while regime 1A corresponds to a D vortex (when the vortex is elongated or far from the pole there is weak wave-1 amplitude and weak winds in *polar* regions). The agree-

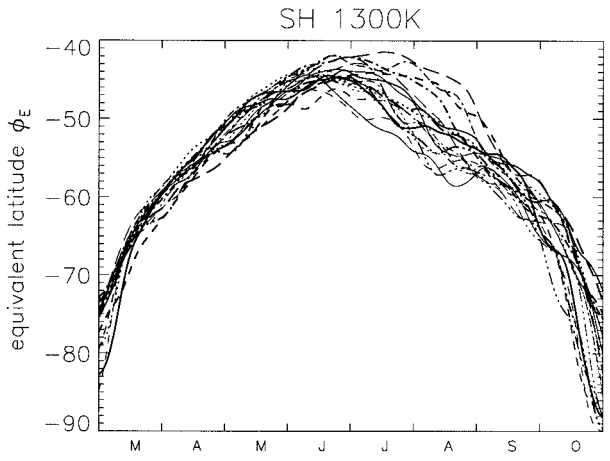

FIG. 15. Temporal variation of φ_E at 1300 K in Southern Hemisphere for each year between 1979 and 1997 (different line type for each year).

ment between the two classifications can be seen by comparing Fig. 14 with Fig. 9 of Pawson and Kubitz (1996) [see also Fig. 11 of Pierce and Fairlie (1993)]. Note that the agreement is not exact and there is often a difference in timing of the two classifications. This is related to the difference in the timing of the zonal wind reversal and mode transition noted by Pierce and Fairlie (1993): the mode transition lags (leads) the wind reversal for wave-1 (-2) warmings.

b. Antarctic vortex

As shown above the interannual variability of the Antarctic vortex at 850 K during early to late winter is small. However, there is large variability in φ_E in the upper stratosphere during midwinter (the interannual standard deviation of φ_E at 1300 K in August is 3.5°). Figure 15 shows that there are years where there is a large vortex (large $|\varphi_E|$) and others with a small vortex, with maximum variability in August. As the polar jet and vortex edge are at approximately the same location [see, e.g., Nash et al. (1996)] this variability in the size of the vortex is consistent with the variability in location of the winter jet at 1 hPa examined by Shiotani et al. (1993). A large (small) vortex corresponds to a low-latitude (high latitude) polar jet. Following Shiotani et al. (1993), we form composites of years with a ''large'' (L) or ''small'' (S) vortex at 1300 K in midwinter; these composites correspond to their low-latitude jet and high-latitude jet composites, respectively. We use φ_E at 1300 K on 1 August to categorize the size of the vortex: a vortex is defined as L if $\varphi_E > -45°$ and S if $\varphi_E < -50°$. With this division there is an L vortex in 1980, 1981, 1987, and 1989, and an S vortex in 1979, 1982, 1985, 1988, 1991, 1992, and 1996. This division into years with an L and an S (and intermediate) vortex is similar to, but not exactly the same as, the division by Shiotani et al. (1993) into low-latitude and high-latitude jet years; L years correspond to the low-latitude jet years of Shiotani et al., but there are some S years that are not high-latitude jet years (1982, 1988) and vice versa (1986).

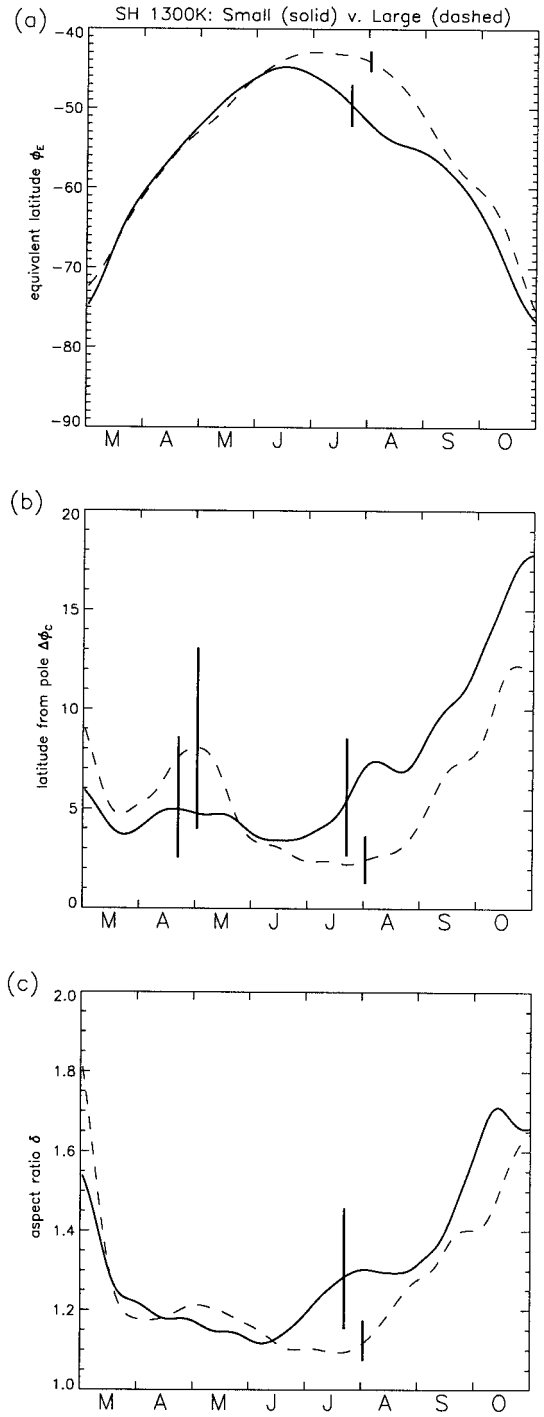

FIG. 16. Temporal variation of (a) φ_E, (a) $\Delta\varphi_C$, and (c) δ at 1300 K for L (dashed curve) and S (solid) composites. The vertical bars represent the range of values within the composites for the given day.

Figure 16 shows φ_E, $\Delta\varphi_C$, and δ for the two com-

posites (the vertical bars represent the range of values within the composites for the given day). There are significant differences between the two composites in the size, the displacement from the pole, and elongation of the vortices during July and August (with vortices in S years being farther from the pole and more elongated), and also a difference in the timing of the minima in $\Delta\varphi_C$ and δ (both occur earlier in S years by over a month). There is also a difference in the location of the vortices, but not the area or elongation of the vortices, in April–May. The above differences between the two composites are consistent with the differences in amplitude of zonal waves 1 and 2 between high- and low-latitude jet years observed by Shiotani et al. (1993).

6. Conclusions

The climatological structure, and interannual variability, of the Antarctic and Arctic polar vortices has been examined using EDs from over 19 yr of PV data. These diagnostics clearly show large interhemispheric differences in the climatological structure of the vortices. The Arctic vortex has a shorter life span (breakdown occurs over a month earlier than the Antarctic vortex), is displaced farther off the pole, and is more elongated (e.g., at 850 K in midwinter, $\Delta\varphi_C \sim 14^\circ$ and $\delta \sim 1.7$ for the Arctic vortex, whereas $\Delta\varphi_C \sim 4^\circ$ and $\delta \sim 1.2$ for the Antarctic vortex). Furthermore, there is a clear midwinter minimum in the distortion of the Antarctic vortex, while the magnitude of the distortion of the Arctic vortex generally increases during its life cycle. There are also large differences in the interannual variability of the vortices: the variability of the Antarctic vortex is small except during the vortex breakdown, whereas the variability of the Arctic vortex is large throughout its life cycle, with the largest variability in late winter (e.g., at 850 K the interannual standard deviation of the midwinter Arctic vortex is three times that of the Antarctic vortex). The large variability of Arctic vortex is due in part to the occurrence of extreme events in which the vortex is very distorted. The evolution of the vortex during these events, which generally correspond to stratospheric warmings, has been examined by isolating periods when the EDs exceed critical values.

The interrelationships of the different EDs (and, hence, characteristics of the vortices) have also been examined. This analysis shows that large displacements off the pole and large elongation of the vortex in the middle and upper stratosphere are both associated with a small vortex. However, there is very little correlation between the displacement off the pole and the elongation of the vortices. Consistent with this, analysis of events when the Arctic vortex is very distorted shows that although the vortex may be well off the pole and elongated within a single event (i.e., within a period of a few days) the extrema in distance off the pole and elongation generally do not occur on the same day.

Many of the features of the ED climatology are consistent with previous climatologies of zonal wave diagnostics. For example, larger amplitude of stationary waves 1 and 2 are observed in the Northern Hemisphere than in the Southern Hemisphere, and there is a midwinter minimum in the amplitude of wave 1 in the Southern Hemisphere (e.g., Randel 1988); both observations are consistent with variations in $\Delta\varphi_c$ and δ shown here. Also, the analysis in section 5 produces results very similar to those of the earlier studies based on wave amplitudes by Pierce and Fairlie (1993) and Shiotani et al. (1993).

However, there are many features that are not apparent in the zonal wave diagnostic climatologies. The maximum displacement of both vortices off the pole occurs at the beginning and end of the vortex life cycle; in contrast, the amplitude of wave 1 in the Southern Hemisphere has maxima in early and late winter (e.g., Randel 1988). There is a midwinter minimum in the elongation of the Antarctic vortex (the minimum in δ occurs around a month before the minima in $\Delta\varphi_c$), but no corresponding midwinter minimum in wave-2 amplitude in the Southern Hemisphere. There are periods when there are large zonal shifts (westward then eastward) in the climatological locations of the vortices: early winter for the Arctic vortex, and late winter to spring for the Antarctic vortex. Also, there are two preferred longitudes of the center of the lower-stratospheric Arctic vortex in early winter (December), and the vortex may move rapidly from one to the other.

There are several aspects of the ED climatology that warrant further study. One is the vertical propagation of disturbances to the vortices. Preliminary analysis using the cross-correlation analysis technique of Randel (1987) shows evidence for the vertical propagation of $\Delta\varphi_C$ and δ with around a 1–3-day lag between 500 and 1300 K, consistent with the zonal wave correlations in that study.

Another area of interest is the link between disturbances to the stratospheric vortex and changes in the tropospheric flow. Preliminary analysis indicates that the observed longitudinal shifts in the center of the lower-stratospheric vortex may be related to changes in the tropospheric circulation. However, more detailed analysis of the structure of the vortex and the tropospheric circulation during these periods is required to confirm this. It will also be interesting to examine in detail the vertical structure of the vortices during events when the vortex is very distorted (e.g., stratospheric warmings). This may provide insight into the relative role of vertical propagation from the troposphere and in situ effects during such events.

The above ED climatology has several possible uses. One obvious use is for comparison with the corresponding diagnostics calculated from numerical models, including multiyear simulations from general circulation models (e.g., The Geophysical Fluid Dynamics Laboratory ''SKYHI'' model; W97), mechanistic model simulations of specific events (such as stratospheric warm-

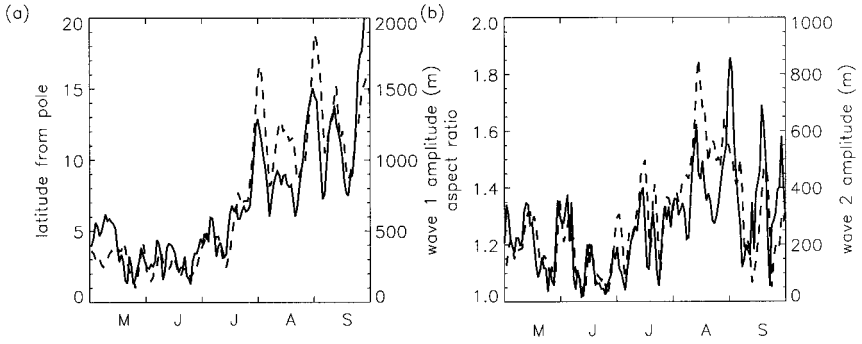

FIG. A1. Temporal variation of (a) wave-1 amplitude at 10 hPa (dashed curve) and $\Delta\varphi_C$ at 850 K (solid), and (b) wave-2 amplitude at 10 hPa (dashed curve) and δ at 850 K (solid) during 1988 Southern Hemisphere winter.

ings), and idealized vortex dynamics models (e.g., Dritschel and Saravanan 1994). These comparisons would complement comparisons of zonal mean and wave diagnostics and would enable the reality of the simulated vortices to be quantified. The ED climatology may also be useful for interpreting satellite measurements of chemical constituents (e.g., measurements from the Total Ozone Mapping Spectrometer and from the Upper Atmosphere Research Satellite). The climatology will also be useful for quantifying how anomalous the vortex structure/evolution is during given years, within the period considered or for later years.

Acknowledgments. This research was supported through the Australian Government Cooperative Research Center Program. WJR is partially supported under NASA Grants W-18181 and W-16215. We thank Gloria Manney for helpful comments on an earlier version of the manuscript.

APPENDIX A

Comparison with Zonal Wave Structure

The relationship between EDs and zonal wave structure (e.g., amplitude and phase of zonal waves) has been examined by W97 for an idealized tracer distribution and for N_2O from the SKYHI general circulation model. Here we examine this relationship for the observed vortices for two periods that highlight the similarities and differences between the two sets of diagnostics.

We consider first the 1988 southern winter. Fig. A1 compares the time series of amplitude of wave 1 (A_1) and wave 2 (A_2) at 60°S of geopotential height at 10 hPa with $\Delta\varphi_C$ and δ at 850 K during June–October 1988. There is a high correlation between A_1 and $\Delta\varphi_C$: both show local maxima or minima on the same days. (Note there is also good agreement between λ_c and the phase of wave 1, not shown.) There is also a high correlation between δ and A_2 except during mid- to late August; during this period the vortex is far from zonal symmetry [i.e., $\Delta\varphi_C$ and δ are large; see, e.g., Fig. 3 of Hirota et al. (1990)]. As the vortex (flow) is far from zonal symmetry linear wave theory breaks down, and changes to A_2 (or A_1) cannot be simply interpreted as changes in the elongation (or position) of the vortex. The above comparison shows that during the periods when the vortex is not significantly distorted (e.g., June–July) there is generally a one-to-one relationship between the EDs and the zonal wave structure, but during periods when the vortex is distorted (e.g., August) this simple relationship breaks down. Note that the 1988 winter was unusually active (with the earliest final warming on record), and the agreement between diagnostics during March–September of other years is usually better.

A more dramatic example of the lack of a simple relationship between the EDs and the zonal wave diagnostics during periods when the vortex is distorted can be seen in Fig. A2, which compares the EDs and wave amplitudes (at 60°N) in the Northern Hemisphere for November–December 1987. During this period the vortex is very distorted: in early December the vortex moves well off the pole, elongates and weakens, and then splits into two parts [see maps of geopotential height and PV shown in Figs. 4 and 7 of Baldwin and Dunkerton (1989)]. This evolution is shown in the EDs: the maximum displacement off the pole occurs around 10 December ($\Delta\varphi_C$ large) and during this time the vortex is very elongated (δ large) (the decrease in vortex size can be seen in the φ_E time series, not shown). However, the wave amplitudes do not even show these features qualitatively. The maximum wave-1 amplitude occurs around a week earlier than the maximum displacement from the pole; the wave-1 amplitude is very small when the vortex displacement from the pole is at its maximum, and the wave-2 amplitude is small during the whole period (note the scale of A_2). The vortex evolution is not captured in the wave amplitudes because during the first half of December the vortex is well off the pole and weakens dramatically, resulting in weak gradients around the 60°N latitude circle (and, hence, weak wave amplitudes).

Comparisons of the two sets of diagnostics for other

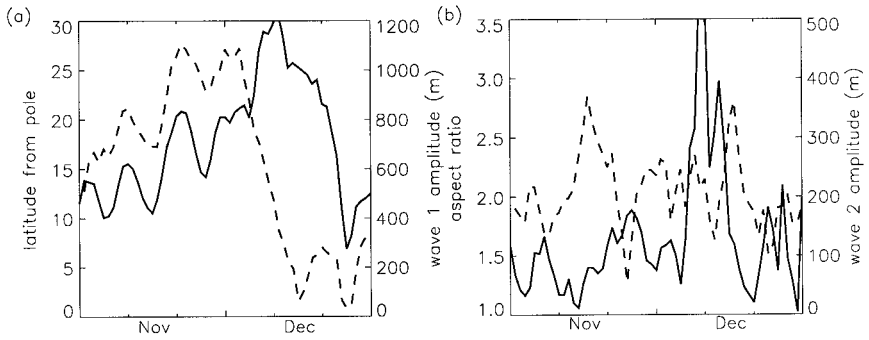

FIG. A2. Temporal variation of (a) wave-1 amplitude at 10 hPa (solid curve) and $\Delta\varphi_C$ at 850 K (dashed), and (b) wave-2 amplitude at 10 hPa (solid curve) and δ at 850 K (dashed) in Northern Hemisphere during Nov–Dec 1987.

years show that there is generally a close relationship between variations in the two sets of diagnostics in the Southern Hemisphere except during the spring breakdown, but poorer agreement in the Northern Hemisphere (where the polar vortex is generally farther from zonal symmetry).

APPENDIX B

Sensitivity to Spatial Resolution and Meteorological Analyses

We examine here the sensitivity of the EDs to the spatial truncation of the NCEP analyses, and the source of the meteorological data. We compare the EDs derived from PV analyses from (i) truncated NCEP analyses, (ii) untruncated NCEP analyses, (iii) the United Kingdom Meteorological Office (UKMO) stratospheric assimilation system (Swinbank and O'Neill 1994), and (iv) the the National Aeronautics and Space Administration/Goddard Space Flight Center (GSFC) data assimilation system (Schubert et al. 1993). Whereas the NCEP analyses are produced using an objective analysis system (Gelman et al. 1986), each of the UKMO and GSFC analyses are from a data assimilation system (in which a global numerical model of the atmosphere is used to provide the first guess field in the assimilation process). Wind and temperature fields are produced directly by these assimilation processes, whereas wind fields have to be derived from the NCEP geopotential analyses (e.g., Randel 1987). The PV is calculated from the UKMO and GSFC wind and temperature fields in the same manner as for the NCEP data. Note that the UKMO and GSFC data are available only for the last 5 or 6 yr, and so (at present) cannot be used to form a long climatology.

We compare here the EDs from the above four PV datasets for the Northern Hemisphere during January 1992. This period was chosen because the evolution during this period has been extensively studied, and because the Arctic vortex is very distorted during this month (e.g., Farman et al. 1994; O'Neill et al. 1994; Plumb et al. 1994; Waugh et al. 1994). In mid-January there was a near-major warming during which the polar vortex moved off the pole in the middle and upper stratosphere. This produced a vortex that tilted equatorward and westward with height (e.g., O'Neill et al. 1994). In late-January the vortex in the lower stratosphere was strongly distorted by a tropospheric blocking event, and there was an intrusion of midlatitude air into the vortex (e.g., Plumb et al. 1994).

Figure B1 compares $\Delta\varphi_C$ and δ for the four different PV analyses at 500, 850, and 1300 K (the same value of PV at each level is used for all analyses). There is good qualitative agreement between the EDs from the different PV analyses, with all showing the same structure and evolution of the vortex during the month. At the beginning of the month the vortex is nearly vertically aligned ($\Delta\varphi_C$ constant with θ), but during the warming event around 10–13 January the vortex slopes equatorward with height ($\Delta\varphi_C$ increases with θ) and the vortex is well off the pole in the upper stratosphere ($\Delta\varphi_C \sim 30°$ at 1300 K). [Note that, consistent with the analysis in previous studies, α decreases with θ (not shown), indicating westward tilt with height.] There are also large changes in the elongation (δ) of the vortex in the middle and upper stratosphere during the warming event. In the lower stratosphere the vortex is nearly circular ($\delta \sim 1$) during first half of the month but is very elongated during last 10 days. The increase in δ around 23 January occurs during the intrusion of midlatitude air into the vortex. During this period the vortex is very distorted in the lower stratosphere and ϵ (the measure of displacement of the PV contour from an ellipse), at 440 and 500 K, is large (not shown), indicating that the vortex shape is nonelliptical, as can be seen, for example, in Figs. 1–4 of Plumb et al. (1994).

Although there is qualitative agreement between the EDs from the different PV datasets there are some quantitative differences. The differences between $\Delta\varphi_C$ derived from the different analyses are generally smaller than 3° (with monthly averaged differences around 1°), with $\Delta\varphi_C$ from the truncated NCEP analyses generally larger than that derived from the other analyses (indi-

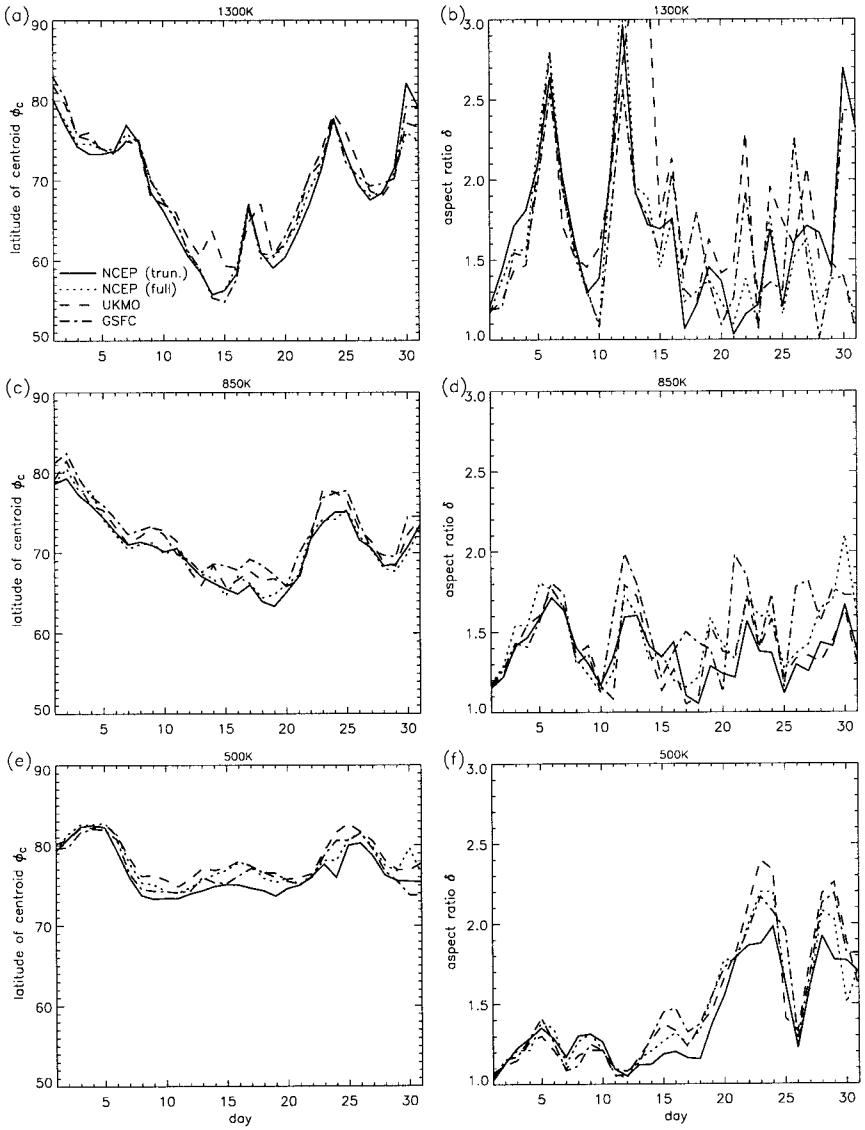

FIG. B1. Evolution of φ_C and δ during Jan 1992 using PV from truncated NCEP (solid curves), untruncated NCEP (dotted), UKMO (dashed), and GSFC (dot–dashed) analyses.

cating that the vortex is farther from the pole in the truncated NCEP analyses). One case where the difference is not small is at 1300 K for 2 days in mid-January, where the difference between φ_C from UKMO PV and that from the other analyses is larger than 5°. The differences between δ from the different analyses are similar to those between φ_C; the differences are small, and the values from the truncated NCEP analyses are generally smaller than from the other analyses (indicating a less elongated vortex). Again there are larger differences at 130 K, particularly between δ from UKMO analyses. These differences in the EDs at 1300 K are consistent with the large differences between the UKMO and NCEP analyses in the upper stratosphere noted by Manney et al. (1996).

The difference between the other EDs calculated from different analyses is also small, except for ϵ. The value of ϵ from the truncated PV analyses is (as might be expected) much smaller than for the untruncated datasets, particularly during periods when the vortex is distorted from zonal symmetry. In W97 it was suggested that ϵ is a good diagnostic for the occurrence of wave-breaking events at the vortex edge, but because of the effect of the spatial truncation on ϵ we do not examine ϵ from the present climatology.

The above comparison indicates that although there

are differences between the EDs from the truncated and untruncated NCEP analyses, these differences are small and similar to the differences between the EDs using PV from different analyses.

REFERENCES

Baldwin, M. P., and J. R. Holton, 1988: Climatology of the stratospheric polar vortex and planetary wave breaking. *J. Atmos. Sci.*, **45,** 1123–1142.

——, and T. J. Dunkerton, 1989: The stratospheric major warming of early December 1987. *J. Atmos. Sci.,* **46,** 2863–2884.

——, and ——, 1998: Biennial, quasi biennial, and decadal oscillation of potential vorticity in the Northern Hemisphere. *J. Geophys. Res.,* **103,** 3919–3928.

Butchart, N., and E. E. Remsberg, 1986: The area of the stratospheric polar vortex as a diagnostic for tracer transport on an isentropic surface. *J. Atmos. Sci.,* **43,** 1319–1339.

Dritschel, D. G., and R. Saravanan, 1994: Three-dimensional quasi-geostrophic contour dynamics, with an application to stratospheric dynamics. *Quart. J. Roy. Meteor. Soc.,* **120,** 1267–1298.

Farman, J. C, A. O'Neill, and R. Swinbank, 1994: The dynamics of the Arctic polar vortex during the EASOE campaign. *Geophys. Res. Lett.,* **21,** 1195–1198.

Gelman, M. E., A. J. Miller, K. W. Johnson, and R. Nagatani, 1986: Detection of long-term trends in global stratospheric temperature from NMC analyses derived from NOAA satellite data. *Adv. Space Res.,* **6,** 17–26.

Hirota, I., K. Kuroi, and M. Shiotani, 1990: Midwinter warming in the southern hemisphere stratosphere in 1988. *Quart. J. Roy. Meteor. Soc.,* **116,** 919–941.

Kalnay, E., and Coauthors, 1996: The NCEP/NCAR 40-Year Reanalysis Project. *Bull. Amer. Meteor. Soc.,* **77,** 437–471.

Lahoz, W. A., and Coauthors, 1996: Vortex dynamics and the evolution of water vapour in the stratosphere of the Southern Hemisphere. *Quart. J. Roy. Meteor. Soc.,* **122,** 423–450.

Lait, L. R., 1994: An alternative form for potential vorticity. *J. Atmos. Sci.,* **51,** 1754–1759.

Livezey, R. A., and K. C. Mo, 1987: Tropical–extratropical teleconnections during the Northern Hemisphere winter. Part II: Relationships between monthly mean Northern Hemisphere circulation patterns and proxies for tropical convection. *Mon. Wea. Rev.,* **115,** 3115–3132.

Manney, G. L., J. D. Farrara, and C. R. Mechoso, 1991: The behavior of wave 2 in the Southern Hemisphere stratosphere during late winter and early spring. *J. Atmos. Sci.,* **48,** 976–998.

——, R. W. Zurek, M. E. Gelman, A. J. Miller, and R. Nagatani, 1994: The anomalous Arctic lower stratospheric polar vortex of 1992–93. *Geophys. Res. Lett.,* **21,** 2405–2408.

——, L. Froidevaux, J. W. Waters, and R. W. Zurek, 1995: Evolution of microwave limb sounder ozone and the polar vortex during winter. *J. Geophys. Res.,* **100,** 2953–2972.

——, R. Swinbank, T. Massie, M. E. Gelman, A. J. Miller, R. Nagatani, A. O'Neill, and R. W. Zurek, 1996: Comparison of UKMO and NMC stratospheric analyses during northern and southern winter. *J. Geophys. Res.,* **101,** 10 311–10 334.

Mechoso, C. R., 1990: The final warming of the stratosphere. *Dynamics, Transport and Photochemistry in the Middle Atmosphere of the Southern Hemisphere,* A. O'Neill, Ed., Kluwer, 55–70.

——, A. O'Neill, V. D. Pope, and J. D. Farrara, 1988: A study of the stratospheric final warming of 1982 in the Southern Hemisphere. *Quart. J. Roy. Meteor. Soc.,* **114,** 1365–1384.

Nash, E. R., P. A. Newman, J. E. Rosenfield, and M. R. Schoeberl, 1996: An objective determination of the polar vortex using Ertel's potential vorticity. *J. Geophys. Res.,* **101,** 9471–9478.

NOAA, 1994: *Climate Diagnostics Bulletin.* Vol. 94, No. 12.

O'Neill, A., and V. D. Pope, 1990: The seasonal evolution of the extra-tropical stratosphere in the Southern and Northern Hemisphere: Systematic changes in potential vorticity and the non-conservative effects of radiation. *Dynamics, Transport and Photochemistry in the Middle Atmosphere of the Southern Hemisphere,* A. O'Neill, Ed., Kluwer, 33–54.

——, W. L. Gross, V. D. Pope, H. Maclean, and R. Swinbank, 1994: Evolution of the stratosphere during northern winter 1991/92 as diagnosed from U.K. Meteorological Office analyses. *J. Atmos. Sci.,* **51,** 2800–2817.

Pawson, S., and T. Kubitz, 1996: Climatology of planetary waves in the northern stratosphere. *J. Geophys. Res.,* **101,** 16 987–16 996.

Pierce, R. B., and T. D. Fairlie, 1993: Observational evidence of preferred flow regimes in the Northern Hemisphere winter stratosphere. *J. Atmos. Sci.,* **50,** 1936–1949.

Plumb, R. A., and Coauthors, 1994: Intrusions into the lower stratospheric arctic vortex during the winter of 1991/92. *J. Geophys. Res.,* **99,** 1089–1106.

Randel, W. J., 1987: A study of planetary waves in the southern winter troposphere and stratosphere. Part I: Wave structure and vertical propagation. *J. Atmos. Sci.,* **44,** 917–935.

——, 1988: The seasonal evolution of planetary waves in the Southern Hemisphere stratosphere and troposphere. *Quart. J. Roy. Meteor. Soc.,* **114,** 1385–1409.

Schubert, S. D., R. B. Rood, and J. Pfaendtner, 1993: An assimilated dataset for earth science applications. *Bull. Amer. Meteor. Soc.,* **74,** 2331–2342.

Shiotani, M., K. Kuroi, and I. Hirota, 1990: Eastward travelling waves in the Southern Hemisphere stratosphere during the spring of 1983. *Quart. J. Roy. Meteor. Soc.,* **116,** 913–927.

——, N. Shimoda, and I. Hirota, 1993: Interannual variability of the stratospheric circulation in the Southern Hemisphere. *Quart J. Roy. Meteor. Soc.,* **119,** 531–546.

Swinbank, R., and A. O'Neill, 1994: A stratosphere–troposphere data assimilation system. *Mon. Wea. Rev.,* **122,** 686–702.

Waugh, D. W., 1997: Elliptical diagnostics of stratospheric polar vortices. *Quart J. Roy. Meteor. Soc.,* **123,** 1725–1748.

——, and Coauthors, 1994: Transport of material out of the stratospheric Arctic vortex by Rossby wave breaking. *J. Geophys. Res.,* **99,** 1071–1088.